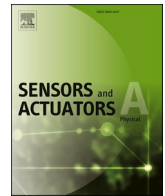Contents lists available at ScienceDirect

Sensors and Actuators: A. Physical

journal homepage: www.journals.elsevier.com/sensors-and-actuators-a-physical

A new planar microwave sensor for fat-measuring of meat based on SRR and periodic EBG structures

Payam Jahangiri, M. Naser-Moghadasi, Behbod Ghalamkari [*], Massoud Dousti

Department of Electrical and Computer Engineering, Science and Research Branch, Islamic Azad University, Tehran, Iran

ARTICLE INFO

ABSTRACT

In this paper, we present a novel microwave sensor for sensing the fat of the meat with high sensitivity. We developed the sensor based on a bent transmission line (TL) and connected it to a split ring resonator (SRR). The gaps in the SRR make hot spots. The material under test (MUT) is placed on the hot spot to increase sensitivity. The sensor is surrounded by electromagnetic bandgap (EBG) elements in the final structure to enhance the Q-factor and save the electric field inside of the sensor. The full-wave simulation resonated with this sensor at triple frequencies of 3.4, 4.08, and 4.55 GHz. Additionally, the proposed EBG unit cell covers 2.4–5 GHz. So, it can make an electromagnetic shield for all resonances, and the final sensor shows dual-band characteristics at 3.48 and 4.67 GHz. The sensor is used to recognize the fat ratio in various meat samples. After Full-wave analysis, the equivalent circuit is extracted and modeled with the aid of an advanced design system (ADS). Next, the relation between the frequency shift of S_{21} nulls and fat percentages is calculated based on a proposed closed-form formula. In the end, comparing full-wave analysis, experimental results, and the equivalent circuit model shows perfect matching.

1. Introduction

The use of microwave techniques for detecting and evaluating material such as fluidic or impurity is a crucial practical concern [1,2]. Much literature has focused on breast cancer tumor detection based on differences between microwave dielectric properties of breast tissues and other parts' permittivity [3]. In addition, the microwave sensor for determining blood glucose levels by permittivity analysis has been documented [4,5]. Other techniques used to model permittivity include substrate integrated waveguide (SIW) cavity and perturbation method [6], passive split ring resonator tag configuration [7], microwave waveguide with FSS [8], cavity method based on perturbation theory [9], interpolation technique based on data organization [10], and reflection/transmission based on Nicolson-Rose method [11]. Still, for highly accurate results, concentrating the electrical field is necessary and has been considered [12]; various methods such as using a split-ring resonator (SRR) [13] and gaps for making hot spots [14] have been studied. Besides, to limit the electric field, the electromagnetic bandgap (EBG) has been developed around the gaps [15]. SRR and EBG are known as conventional types of metamaterials. These metamaterial structures have been noticed for their left-hand characteristic in the

microwave regimes to manipulate the electromagnetic wave for various applications including sensing as the metasurface [16,17] and electric field shielding for reducing mutual coupling [18]. Diverse metamaterial structures have been developed as defected ground structures, like split-ring resonators as a complementary formation [19]. Recently, metamaterial in various models has been developed for designing novel sensors based on the outer material effect on the capacitance to make frequency shift for proximity microwave sensors [20,21].

The microwave sensors were employed for various industrial applications, such as determining the alcohol percentage [22] and industrial oil life [23]. Moreover, Ghatass et al. determined the dielectric properties of the meat by measuring the capacitance and conductance of meat with two parallel silver-plated electrodes [24]. Sing et al. use the waveguide method to determine the added fat in meat paste [25]. They applied their method to beef meat to evaluate fat and salt [26,27]. Notably, in their method, the whole waveguide should be filled with the sample, and using a piece of meat for fat determination is not possible. Jilani et al. use a bulky single resonance planar microwave sensor for determining the fat percentage of chicken meat [28]. Three types of techniques have mainly been developed for designing the microwave sensor for liquid and dielectric sensing, including parasitic elements

[29], making a cavity in connection with a transmission line [30], and coupling between two cavities [31].

In this paper, we designed a small dual-band planar sensor to determine the fat percentage of meat. First, we introduced a particular transmission line with an internal loop and gap. The structure has rejection frequencies at 3.4, 4.08, and 4.55 GHz. Second, a shielding model based on EBG is developed to concentrate the electric field in the sensor to improve the resolution. This structure is helpful for proximate sensor design, and the frequency shift is considered for material detection. The circuit model (CM) is extracted for the proposed structure to confirm the simulation results. Accordingly, we suggest the bent transmission line as the proposed sensor to be used as a proximate sensor or imported into liquids or meat for measuring the determined unique features. The value of the Q-factor, the operation frequency, and the magnitude value of S_{21} are considered for recognizing various fat levels.

This study is organized as follows: Section II presents the design and modelling of the proposed sensor. Section III illustrates the calculation of the circuit model of the sensor. Section IV provides the numerical results for the designed sensor, and the finite element method (FEM) carried out to validate the formulations of the circuit model plus parameter studies. The fabricated sensor, experimental results, and closed-form formula for sensing are provided in section V. Finally, section VI presents the study conclusion.

2. Design and modelling of the sensor

In previous studies, SRR and CSRR structures have been used as parasitic elements [29,30]. These methods have two major drawbacks: 1) the dimensions of the structure usually become larger, and 2) the field in the parasitic element must be increased to create resonance, and this coupling reduces the field; therefore, the Q-factor will reduce. To overcome these two challenges, we used a curved transmission line, and then instead of using a parasitic element, we used SRR inside the line. Furthermore, the equivalent circuit shows us what the role of the gaps is, and by controlling the gaps, we can control the capacitors and thus increase the storage field.

The proposed sensor is developed in two steps. In the first step (Step 1), a microwave sensor (filter) based on a split-ring resonator (SRR) is designed as the primary structure, and in the second step (Step 2); it is surrounded by EBG structures to concentrate the electric field to reduce the electric field losses. In the first structure, the bent transmission line is considered to reduce the dimension of the proposed sensor. The total size of the proposed sensor is 42.5×38 mm^2. The used substrate is Roger-RO4003 with a thickness of 0.8 mm, a permittivity of 3.55, and a loss tangent of 0.0027. As shown in Fig. 1, the gaps in the SRR play a critical role in making the hot spot and resonances by adding some shunt capacitances [32]. The MUT (the meat with various fat percentages) samples can be placed over the central rectangular section. The TLs are connected to a 50 Ω SMA to excite the proposed sensor.

The proposed EBG unit cell is depicted in Fig. 2(a). The meandered structure is used to decrease the operating frequency of the unit cell in comparison with the basic model of the EBG. As Fig. 2(b) shows, the meandered line increases the cell inductance, and thus, the frequency shifts to the lower frequency, so the bandgap is between 2.4 and 5 GHz. The bandgap of the EBG unit cell is modified for the frequency range of the proposed sensor and helps to increase the energy and Q-factor of the sensor.

The CRLH (Composite Right/Left Hand) circuit includes right-hand and left-hand elements, including series and shunts inductance and capacitances, and interaction between these elements makes various frequencies. Here, the first mode is related to $\omega_M = 1/\sqrt{L_R C_L}$ and the second mode can be calculated by $\omega_E = 1/\sqrt{L_L C_R}$, and thus, the composite structure frequency can be calculated by $f_0 = 1/2\pi\sqrt{L_R C_L L_L C_R}$.
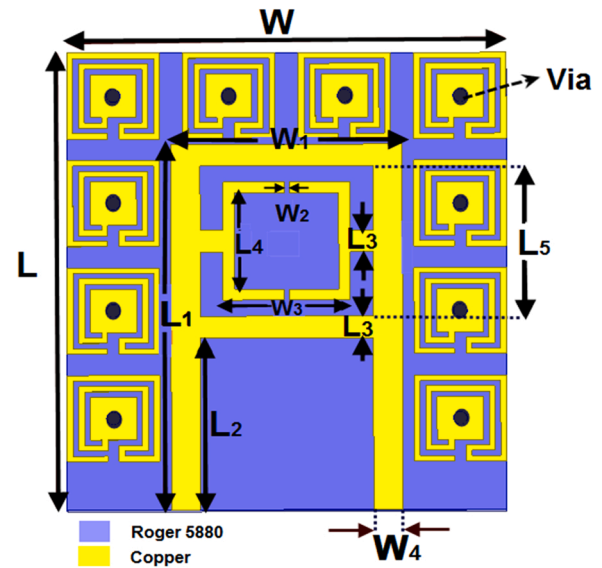

Fig. 1. the schematic of proposed sensor where W = 38 mm, L = 42.5 mm, W$_1$ = 20 mm, W$_2$ = 0.5 mm, W$_3$ = 11 mm, W$_4$ = 2.5 mm, L$_1$ = 34 mm, L$_2$ = 16 mm, L$_3$ = 2 mm, L$_4$ = 9 mm, L$_5$ = 14 mm.
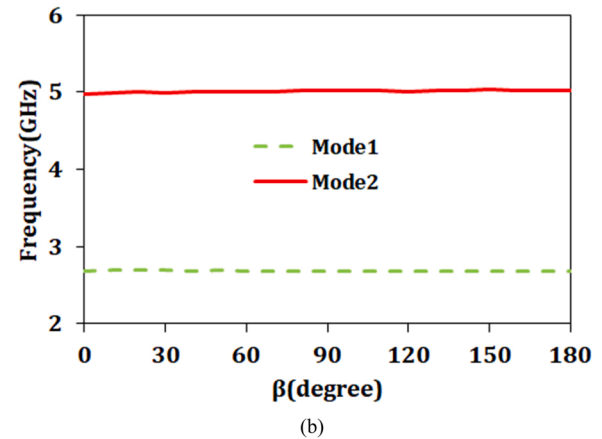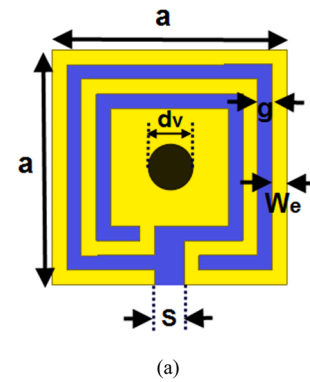
Fig. 2. (a) The schematic unit cell of the proposed EBG where a= 8 mm, g= 0.5 mm, We= 0.5 mm, S= 1 mm, dv= 1.2 mm (b) Dispersion diagram for the EBG cell.

3. The circuit model for the proposed sensor

The extended circuit model for the proposed sensor is presented in Fig. 3. Eq.1 to 8 extracts the circuit model parameters [33,34]. As shown in Fig. 3, every transmission line is modeled with the π-form circuit, which contains inductance and two parallel capacitors [35,36]. So, the
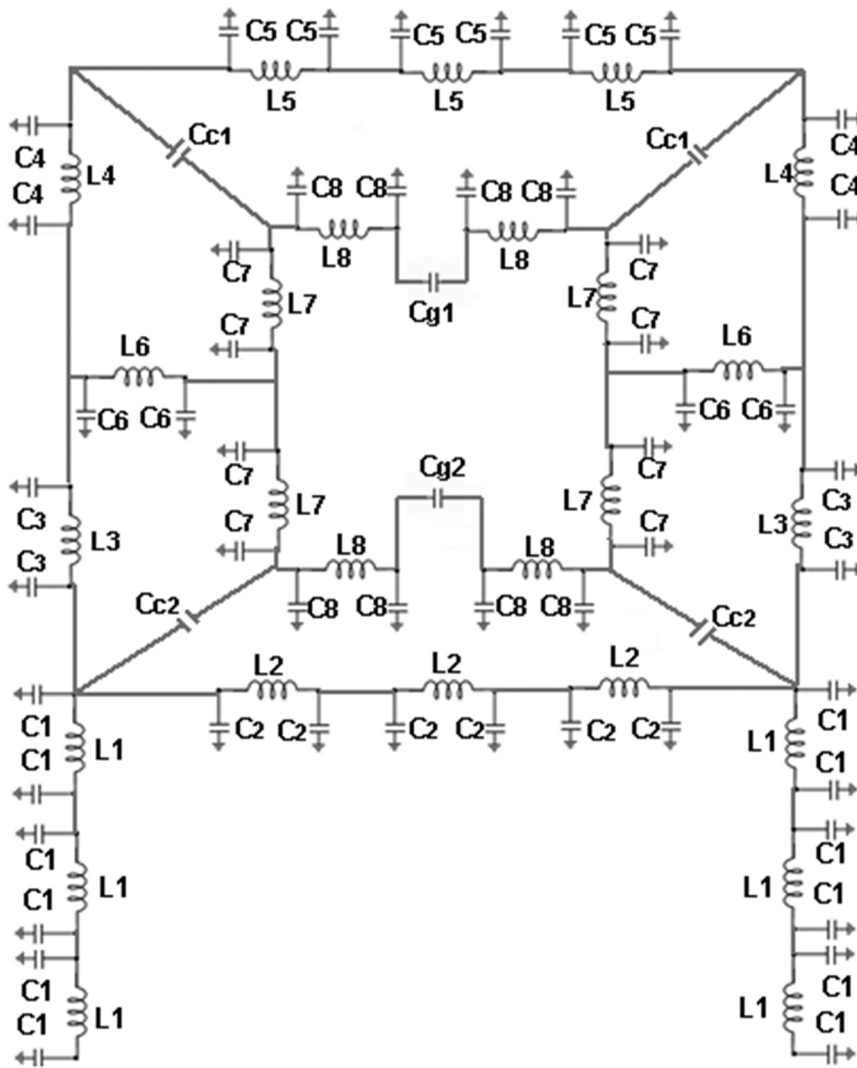
Fig. 3. Equivalent circuit model $L_1 = 0.98$ nH, $L_2 = 0.99$ nH, $L_3 = 1.5$ nH, $L_4 = 1.32$ nH, $L_5 = 1.45$ nH, $L_6 = 0.47$ nH, $L_7 = 0.95$ nH, $L_8 = 1.64$ nH, $C_1 = 0.26$ pF, $C_2 = 0.2$ pF, $C_3 = 0.36$ pF, $C_4 = 0.32$ pF, $C_5 = 0.28$ pF, $C_6 = 0.11$ pF, $C_7 = 0.09$ pF, $C_8 = 0.13$ pF, $C_{g1} = 0.08$ pF, $C_{g2} = 0.1$ pF, $C_{c1} = 0.03$ pF, $C_{c2} = 0.05$ pF.

inductance can be obtained by Eq.1. The capacitance of the TL can be calculated by Eq.5. In this structure, two types of gap capacitors are used, playing an essential role in controlling the operation frequency. The first capacitors are placed between the inner and outer loops (C_{c2} and C_{c1}). The second ones are placed at the center of the inner loop (C_{g1} and C_{g2}), and the capacitor of the gaps can be obtained by Eq.9.

The inductance of the TL line can be obtained by Eq.1, where the l is the length of the transmission line, w is the width, and t shows the thickness of the line. Here, K_g can be calculated by Eq.2, and h is the thickness of the substrate.

$$L(nH) = 2 \times 10^{-4} l \quad \left[ln\left(\frac{l}{w+t}\right) + 1.1 + \frac{w+t}{3l} \right].K_g \tag{1}$$

$$K_g = 0.57 - 0.145 \quad ln\left(\frac{w}{h}\right) \quad for \quad \left(\frac{w}{h} > 0.05\right) \tag{2}$$

The resistance of the transmission lines can be calculated using Eq.3, where R_{sh} is the impedance of the sheet resistance per square meter of the conductor, *and* l is the length of the transmission line. *In* Eq. 4, K is the known factor for the width ratio over the thickness of copper. Since the R value is insignificant, it is ignored in the CM and assumed lossless.

$$R_s(\Omega) = \frac{KR_{sh}l}{2(w+t)} \tag{3}$$

$$K = 1.4 + 0.217 \quad ln\left(\frac{w}{5t}\right) \quad for \quad \left(5 < \frac{w}{t} < 100\right) \tag{4}$$

The gap capacitance for the microstrip structure can be obtained by Eqs. 5 to 6 based on the even and odd analysis [35]:

$$C_1 = 0.5C_{even} \tag{5}$$

$$C_2 = 0.5C_{odd} - 0.25C_{even} \tag{6}$$

4. Simulation results of the sensor and discussions

Fig. 4 depicts the insertion loss of the proposed structure with and without EBG (a). Based on Fig. 4(a), the sensor is a triple-band resonator. Simulation is done with HFSS as full-wave commercial software, and the result is compared with the circuit model of ADS in Fig. 4(b). The first resonance occurs at 3.4 GHz, the second one happens at 4.08 GHz, and the third one at 4.55 GHz. Using the EBG structure, the Q-factor at the first frequency will increase, and the transmission reduces; however, at a higher frequency, the EBG hurts the resonance shape and Q-factor. Notably, a good agreement between the two methods is evident. The resonator Q-factor is positively related to the stored energy in the device as shown in Eq.7 and can be calculated by Eq.8 [37]:
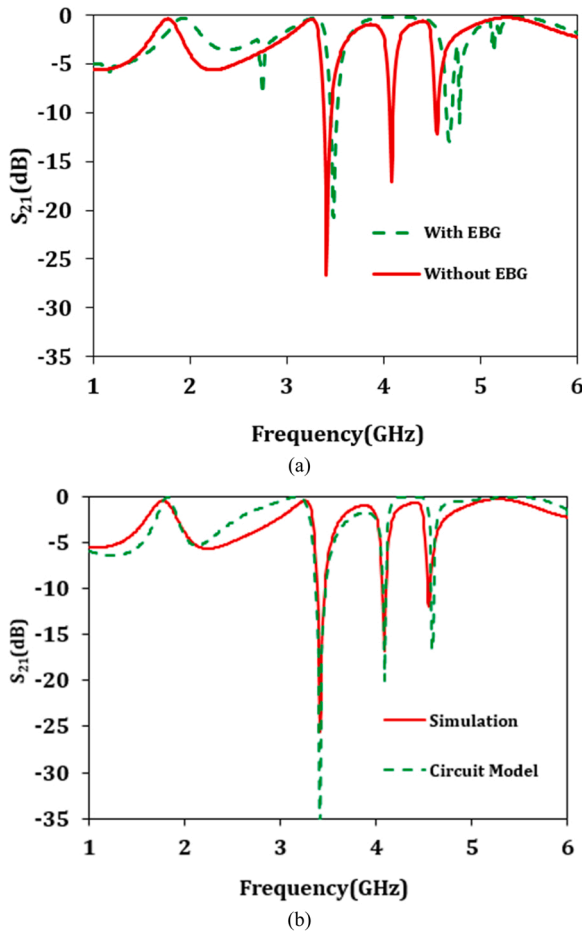
3

(a)

(b)

Fig. 4. The transmission of the sensor (a) without sample with EBG and primary structure(b) the equivalent circuit model and simulation result comparison for the primary filter.

$$Q = 2\pi f_r \times \frac{energy\ stored}{Power\ loss} \tag{7}$$

$$Q = \frac{f_0}{BW_{3dB}} \tag{8}$$

Thus, the Q- factor of the proposed sensor is 386 and 93 for the first and second resonances. Plus, for the primary sensor, the Q-factor is 254, 204, and 90 for the first, second, and third resonance, respectively. As Fig. 5 illustrates, the EBG helps the sensor Q-factor of the sensor increase and the energy concentration. Simply put, the higher Q-factor saved more energy in the proposed sensor and a slight change in the material, and permittivity can increase the frequency shift essential for recognizing the unknown material.

In short, the use of EBG had several functions in the proposed structure. Due to the limited distance between the elements and the structure, the shielding effects are limited, and the coupling is also effective, but in the end, the maximum amount of energy has increased. However, the effects on the Q-Factor level were not significant. Nevertheless, EBG use caused the second resonance removal, which makes the main resonance examined with test materials without disturbance.

The electric field can be studied to realize the effect of each element on the sensor response. Then, in Fig. 5, we examined the electric field for the proposed sensor in the presence or absence of the EBG considering both resonances. As Fig. 5 shows, using the EBG shield, the maximum value of the electric field on the sensor's surface reveals a significant enhancement. For the first resonance, as shown in Fig. 5(a), the sensor without EBG has the maximum E-field value of 1.65E+ 4, and also, for

the sensor with EBG at this frequency, this value is 6.04E+ 4 (Fig. 5(b)). In other words, we can see more than 360 % enhancement in the electric field. As shown in Fig. 5(c), in the second resonance, for the primary structure, the maximum value of the E-field is about 9.29E+ 4, and for the proposed design, it is intensified to 1.10E+ 5 (Fig. 5(d)). Here, the same as the first resonance, we have more than 115 % enhancement of the E-field by using the EBG arrays. Finally, the maximum E-field value equals 5.11E+ 4 for the primary structure of the third resonance, shown in Fig. 5(e).

The proposed sensor determines the ratio of fat in meat for industrial applications. Different factors can affect the effective permittivity of the meat, such as moisture and fat percentage [38]. So, the transmission of the proposed sensor for different permittivity values is checked, and the results are presented in Fig. 6(a). The permittivity of the meat is assumed to be 10–50 for the constant loss tangent of 0.32. By increasing the permittivity, the resonances shift to a lower frequency. The transmission value (magnitude of S_{21}) for the higher resonance shows reduction such as 4.67 GHz, where the value from −11 dB for $\varepsilon = 10$ changes to −25 dB for $\varepsilon = 50$ but the resonances at 3.48 GHz, the transmission changes from −20 dB for $\varepsilon = 10$ changes to −7 dB for $\varepsilon = 50$. In Fig. 6(b), the transmission of the sensor is checked for various loss tangents in the range of 0.06–0.36 for a constant permittivity of 22. The results show that the transmission value changes nonlinearly but typically. By increasing the loss tangent, the value of the transmission increases. In general, it can be analyzed as a narrow band, but in the case of materials that are used, such as alcohol or meat, which have a non-linear behavior, a wide band can be considered a tool for understanding non-linear behaviors at higher frequencies. In addition, the multiband structure can be used for increasing the sensing by increasing the information on each resonance, as shown in this study.

The effective permittivity of the sample can be obtained by the Maxwell-Garnett as shown in Eq. 9, where ε_{eff} is the complex permittivity of the sample and *f* is the fraction ratio. Here, ε_s is the permittivity of the added material, which is fat here, and ε is the permittivity of the host material, which is the meat [39].

$$\varepsilon_{eff} = \varepsilon + 3f\varepsilon\frac{\varepsilon_s - \varepsilon}{\varepsilon_s + 2\varepsilon - (\varepsilon_s - \varepsilon)f} = \varepsilon\frac{2(1-f)\varepsilon + (1+2f)\varepsilon_s}{(2+f)\varepsilon + (1-f)\varepsilon_s} \tag{9}$$

The permittivity of the perfect meat is about 47 +j18.5, and the permittivity of the fat in the range of 1–7 GHz can be supposed to be 3 +j1. Thus, based on Eq. 23, the permittivity of the sample is shown in Table 1. Here, the result from Maxwell-Garnett is compared with the experimental result in [27]. The results show good agreement between calculation and the data presented in [27] when the fat percentage is less than 20 %. However, by increasing the fat to 30 %, the permittivity shows nonlinear behavior. The values of the Table1 are used for sample simulation in HFSS software. Even though the permittivity of fat is lower than that of meat, it has a higher imaginary permittivity ratio to the real part. As shown in Table 1, with the increase in fat percentage, the structure becomes more lossy, and this is due to the presence of more O-H junctions of water in fats because of hydrophilic lipids head of them [40]. As a result, alcohol, and water are stored more in these tissues. Therefore, when the fat percentage changes, it creates a non-linear state.

The transmissions (S_{21}) of the proposed sensor are presented in Fig. 7 for various types of meat with different fat percentages for three different types of substrate. The sample with the dimension of $20 \times 14 \times 3$ mm^3 is placed on the inner ring. The permittivity of the meat with varying rates of fat is selected as it has been reported in [27]. As shown in Fig. 7, the sample causes a frequency shift at both frequencies. Notably, another critical factor is the Q-factor of the resonance. At the first resonance, the frequency shift difference between various samples is not too much. The magnitude of S_{21} change is visible, and in the second resonance, both frequency shifts and the magnitude of S_{21} variation can be seen. In fact, by increasing the fat percentage, the loss effect increases. In Fig. 7(a), for the substrate of Ro-4003, for the meat with the 3 % fat, the first and second resonances occur at 1.69 and
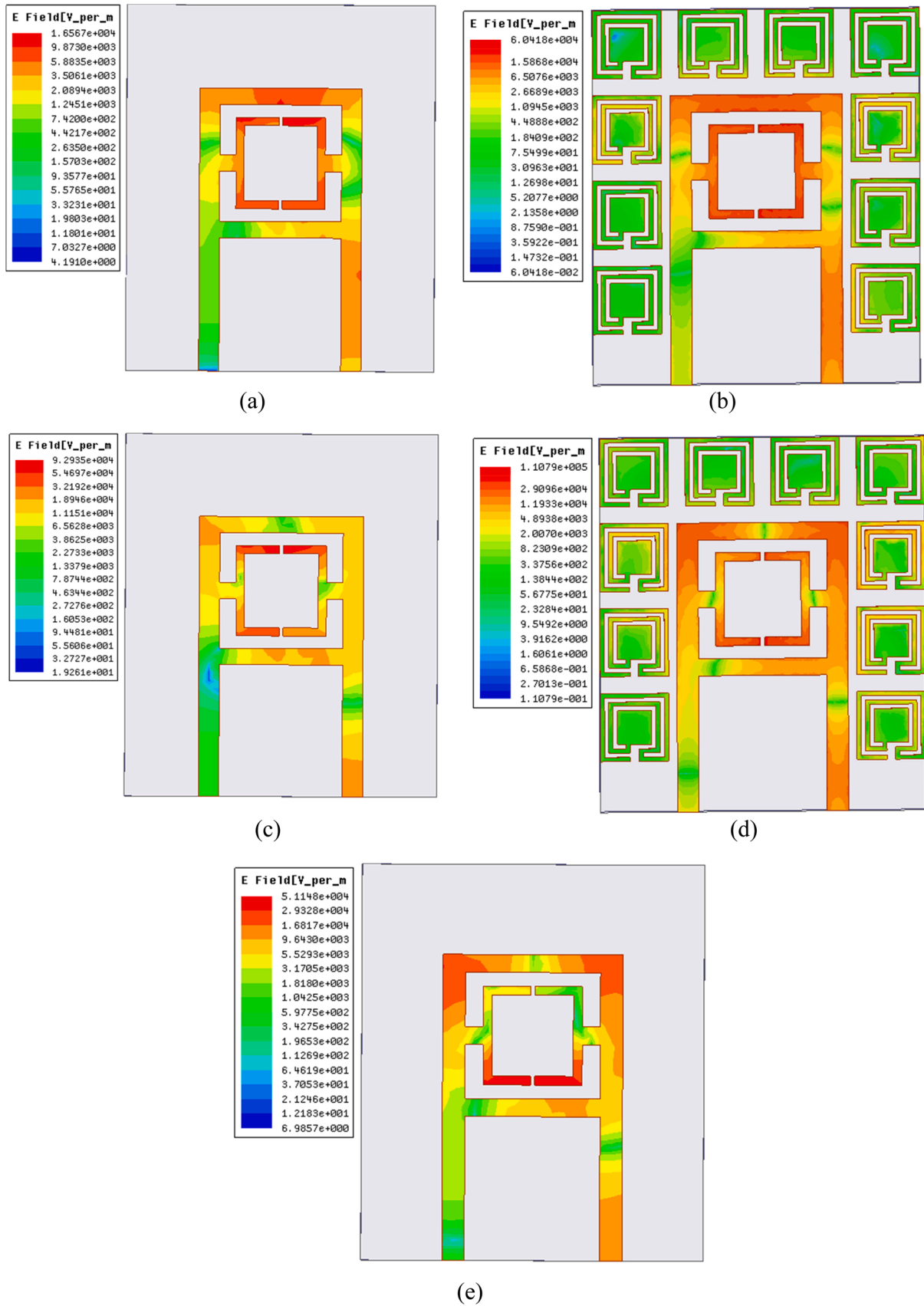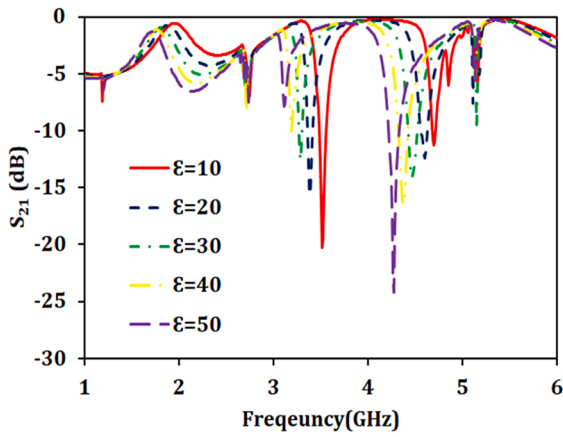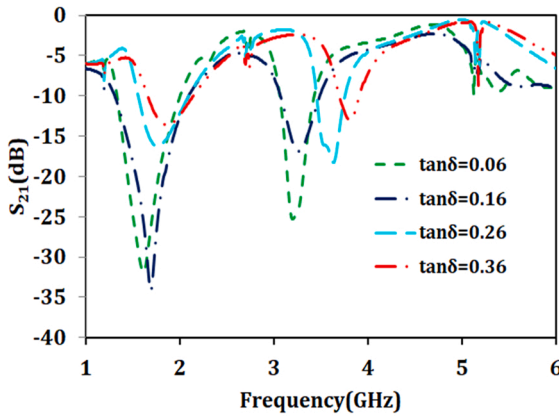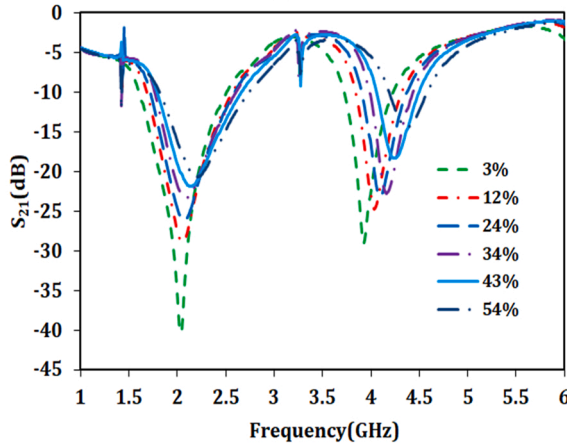
Fig. 5. The electric field distribution of the sensor (a) without EBG at 3.41 GHz (b) with EBG at 3.48 GHz(c) without EBG at 4.08 GHz (d) with EBG at 4.67 GHz (e) without EBG at 4.54 GHz.

(a)

(b)

(c)

Fig. 6. (a) The transmission of the sensor with samples (a) study the effect of the permittivity (b) study of the loss tangent of MUT.

Table1
The real and imaginary permittivity of the meat with various percentages of fat by Maxwell-Garnett and experimental results of [27].

	3 %	12 %	24 %	34 %	43 %	54 %
Permittivity Real Ref. [38]	46.7	42	37.5	22.7	14	10.5
Permittivity Real calculation	45.1	39.7	33.15	28.16	23	19.25
Permittivity Imaginary Ref. [38]	18.25	14.9	13.1	6.1	3	2
Permittivity Imaginary calculation	17.75	15.6	12.97	10.9	9.3	7.44

(a)

(b)

Fig. 7. Transmissions of the proposed sensor for first and second resonances (a) for Ro-4003 (b) for FR-4 (c) Ro-5880.
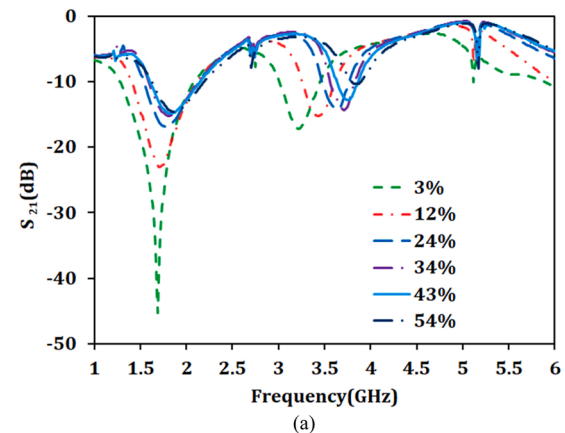
3.2 GHz with values of −45 and −17 dB, and by increasing the fat level to 54 %, the first and second resonances occur at 1.85 and 3.8 GHz with values of −14 and −10 dB. In Fig. 7(b) and (c), the results are checked for FR-4 and Ro-5880 as the substrate of the proposed sensor. The results show that lossy substrates such as FR-4 can increase the losses of the sensor and cause a reduction of the Q-factor, and also shifts the operation frequency to lower frequencies. On the other hand, the lower loss of the Ro-5880 causes the increase in the Q-factor mostly in the second resonances, and also, its lower permittivity causes increasing the operation frequency of the sensor.

By looking at Table 1, we can see that the increase in the amount of fat in compression with meat, the amount of imaginary permittivity, or the losses relative to the real permittivity increases. As a result, the
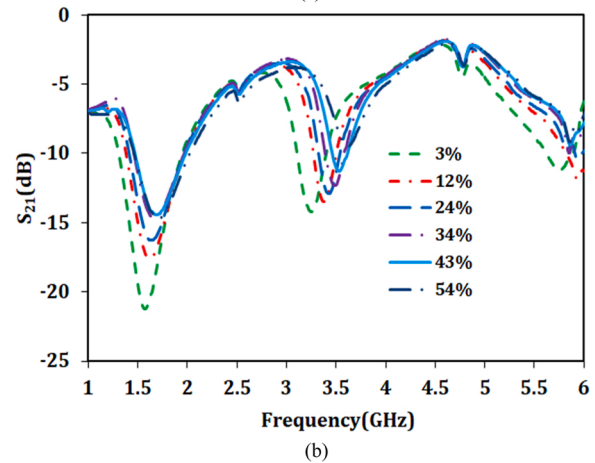
material becomes more lossy, so the wave hitting the object becomes a loss. In practice, it works like a short circuit, and this short circuit will improve by increasing the fat percentage.

5. The experimental result, material sense, and proposed closed-form formula

Fig. 8(a) shows the fabricated sensor with the EBG unit cells, and the measurement setup is presented in Fig. 8(b). We employed the network analyzer (Agilent-8722ES) for calculating s-parameters and probed the meat with different fat percentages with the proposed sensor. Fig. 8(c) illustrates different meat samples used for measurement.

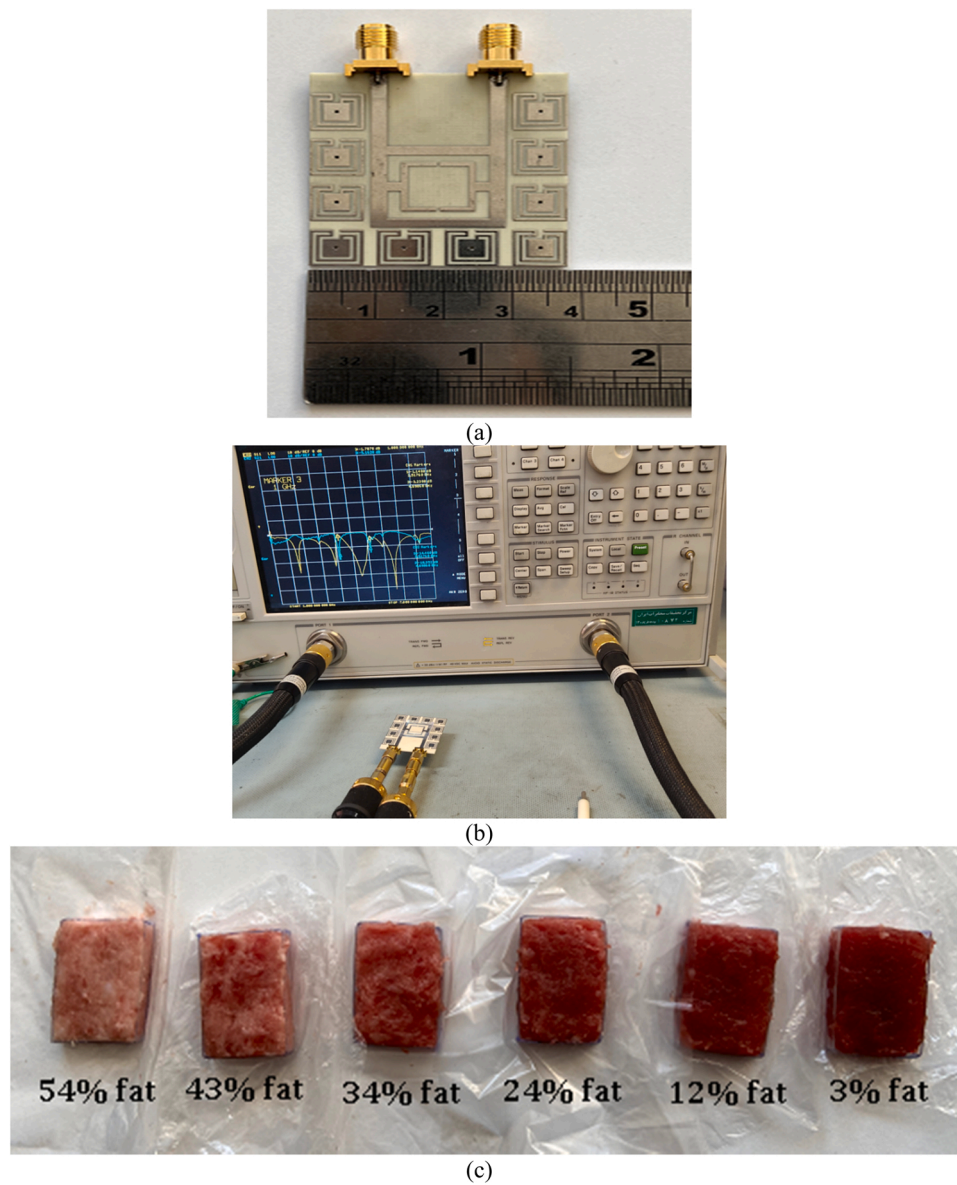Fig. 9 depicts the transmission of the proposed fabricated sensor. A

(a)

(b)

(c)

Fig. 8. (a) The proposed fabricated sensor (b) the measurement set up (c) various samples of meat with different levels of fat from 3 % to 54 %.
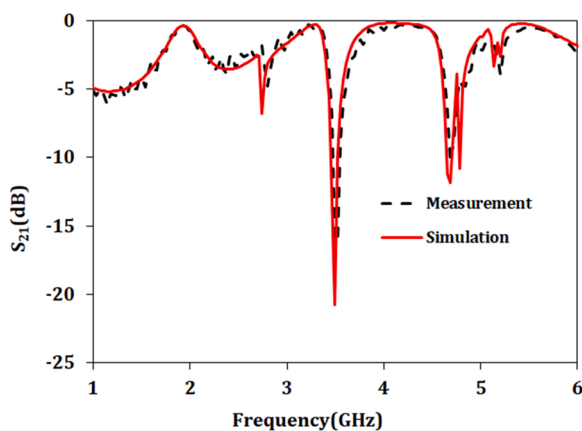

Fig. 9. comparison between S_{21} of the simulation and experimental.

perfect similarity can be seen between simulation and fabricated sensors. Generally, we are dealing with non-linear materials considered ideal in the simulation environment, which can cause a difference between simulation and experimental (see Table 1). In the software, we usually overlook the currents caused by environmental situation, but in the practice, the physical conditions of the test environment and the final quality of the element under test play important roles. For sure, in the simulation, metals are considered as PEC and without thickness.

To test the meat with various fat percentages, we selected 0.005 Kg samples with the dimension of $20 \times 14 \times 3$ mm^3 as used for simulation. The temperature of the environment is considered 27 °C. Comparing the simulation result in Fig. 7 and experimental measurement in Fig. 10 concludes that a good agreement between the two cases is evident. However, some other parameters, such as loss of connector and the environmental condition, cause the reduction in the transmission (S_{21}) of the experiment. In this study, we did not explore the humidity and temperature. Nevertheless, as mentioned above, fat is much more hydrophilic than meat, so when the ratio of fat in meat increases. We see an intensifying in the imaginary part of the permittivity caused by more water and alcoholic compounds.
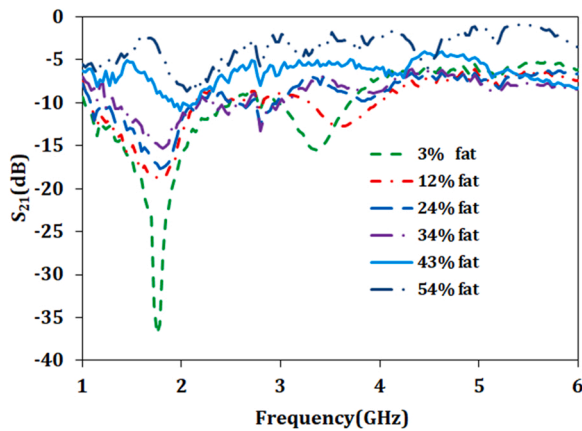
Fig. 10. The transmission of the proposed sensor (S_{21}) for various samples while the level of the fat is changed.

The main goal of designing a microwave sensor is to recognize unknown materials based on the electrical characteristic of the materials that affect various parameters of the sensor, such as frequency shift and phase variation. Here, we considered the frequency shift, amplitude change, and the Q-factor for both resonances to recognize the fat percentage in samples. As Table 2 shows, a good similarity can be seen between simulation and experimental results for operation frequency. In addition, it is visible that the second resonance difference between frequencies is about 1.11 GHz for the experiment, and it is more than the first resonance, which is about 0.4 GHz, which means that the second resonance has a better resolution for detecting the fat percentage based on frequency shift. So, the second resonance is more suitable for obtaining the unknown material based on frequency shift. This different behavior of each resonance is oriented from the capacitors and inductors made by the transmission line and gaps. Therefore, in each resonance, some interact with MUT. On the other hand, in Table 3, the Q-factor of both resonances is checked. The first resonance has a higher Q-factor and the variation of the Q-factor by changing the fat percentage is visible. Then, the first resonance can detect the unknown material based on the Q-factor. As a result, the multi-band characteristic behavior of this sensor helps us to recognize the effect of frequency shift at the second resonance and Q-factor of the first resonance to increase the quality of the sensing. When the materials under test are lossy, the ratio of the loss field to the stored field increases. Consequently, we see a decrease in the Q-Factor. Yet, in structures where the material under test is highly lossy, it is not possible to check the frequency shift in many cases, or it does not show a wide separation, so in such cases, the use of q-factor is much more practical.

The comparison between resonate frequency shift ($\Delta f = f_{sam} - f_0$) and amplitude for the second resonance are presented in Fig. 11 (a) and (b), respectively. Both simulation and experimental results have linear variation, which makes this sensor suitable for detecting unknown percentages of fat.

In brief, the working frequency of the structure shifts to lower frequencies when the material under test is placed on it, which is due to the increase of the sensor's external capacitor. Nonetheless, assuming that

Table 2

simulation and experimental frequencies for the various percentages of the fat.

	Simulation		Experimental	
	$f_1(GHz)$	$f_2(GHz)$	$f_1(GHz)$	$f_2(GHz)$
3 %	1.69	3.21	1.75	3.37
12 %	1.71	3.44	1.77	3.64
24 %	1.78	3.62	1.81	3.82
34 %	1.81	3.72	1.83	3.94
43 %	1.83	3.77	1.99	4.12
54 %	1.86	3.85	2.15	4.48

Table 3

Q-factor of both frequencies for simulation and experimental for the various fat percentages.

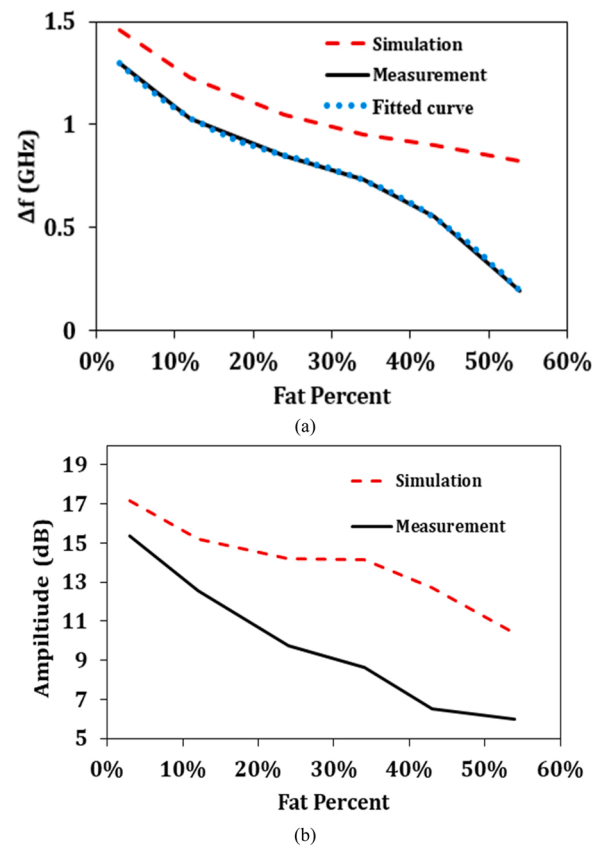|	Simulation		Experimental	
	$f_1(GHz)$	$f_2(GHz)$	$f_1(GHz)$	$f_2(GHz)$
3 %	56.3	13.65	26.11	8.4
12 %	8.53	13.5	4.27	4.9
24 %	5.26	15.21	5.01	4.44
34 %	4.48	22.76	4.35	0
43 %	4.7	15.86	3.13	0
54 %	4.37	11.46	3.85	14.9

(a)

(b)

Fig. 11. comparison between simulation and experimental (a) resonate frequency shift (b) the amplitude of the S_{21}.

the permittivity is uniform in the desired spectrum, we see different behavior in the two frequencies. This difference is due to the difference in the elements producing resonance and the mutual interaction of the material under test and the desired structure. The first frequency is mainly created by the gap capacitors in the center, but the gap capacitors producing the second resonance are smaller, and the effect of inductors is more effective in transmission lines. So, it can be said that at high frequencies, the inductance property created by the material under test is the most effective factor, and at low frequencies, the capacitance, so this effect can be seen in the Q-factor. On the other hand, at higher frequencies, there is an equal change in the number of capacitors and inductors compared to the lower frequency, which is equivalent to a larger ratio in the total capacitor and inductor, so the frequency shift occurs more.

Finally, Lagrange interpolation was used for calculating the percentage of the fat in the samples based on Fig. 11 (a) for the experimental results. Eqs. 10 and 11 introduce Lagrange interpolation as follows:

$$P(x) = \sum_{j=1}^{n} P_j(x) \tag{10}$$

$$P_j(x) = y_j \prod_{k=1; k \neq j}^{n} \left(\frac{x - x_k}{x_j - x_k} \right) \tag{11}$$

Here x and y are for the Cartesian coordinate system [15], and $P(x)$ is a frequency-based function. Thus, it is possible to predict the fat percentage for the material under test (MUT). The value of $P(x)$ is presented with Eq. 12, and here, the fifth-order equation is obtained for higher accuracy.

$$P = 4.72 \times 10^{-9}(\Delta f)^5 - 5.3 \times 10^{-7}(\Delta f)^4 +$$
$$3.09 \times 10^{-6}(\Delta f)^3 + 1 \times 10^{-3}(\Delta f)^2 \tag{12}$$
$$-4.5 \times 10^{-2}\Delta f + 1.42$$

As shown in Fig. 11 (a), the Fitted curve is the same as the measurement, and here, the SSE (sum square error) is obtained as 7.6E-30.

The comparisons of the proposed sensor with previous models are presented in Table 4. Here, the type of sensor, type of material, size of the sensor, operating frequency, and Q-factor are compared. The various sensors like a transmission line with a split ring, a transmission line with a gap, and a waveguide with FSS and SIW are considered for this comparison. This comparison shows that the proposed sensor in this study has a higher Q-factor of 386 while the SIW cavity with a similar frequency has a lower Q-factor ($\sim$160), and using a substrate with higher permittivity ($\varepsilon_r = 10$), results in reducing the size of the cavity to 35×20 mm^2. The waveguide sensor with FSS is a complicated technique. The size of FSS is 22.8×10.1 mm^2, but here, we ignored the size of the waveguide, and in this model, putting a sample in the holder is very hard. In some other studies, parasitic elements [29], making a cavity in connection with a transmission line [30], and coupling between two cavities [31] have been noticed. However, as shown in the Table4, the parasitic element [29] and making a cavity in connection with the transmission line [30] has a low Q-factor, and in the coupling between two cavities [31], the S_{11} and S_{22} are used for measurement which is not interesting for sensing because typically the S_{11} is equal with S_{22}.

6. Conclusion

A microwave sensor based on a split ring resonator was developed in this paper. Using the SRR and bent transmission line, the structure was made compact more than the previously studied model, and it shows dual-band characteristics at 3.48 and 4.67 GHz. The results show the effect of the EBG unit cell for controlling the electric field up to 470 %, and the Q-factor is increased from 254 for the sensor without EBG to 386 for the contained EBG model. The equivalent circuit for the proposed sensor was extracted and compared with a full-wave simulation to show the effect of the elements in this sensor. The effect of materials with different permittivity and loss-tangents was examined to reveal their effect on the sensor's response. The proposed structure was used for checking the level of fat in the meat, and the result shows that, for the first resonance, the effect of the meat and fat permittivity on the Q-factor can be considered as the factor for recognizing the percentage of the fat, and for the second resonance the frequency shift and sensitivity are more acceptable. In addition, the Maxwell-Garnet model was used for modelling and obtaining the real and imaginary part of permittivity to have an accurate model for materials under test. Finally, the experimental, circuit model, and simulation results were compared, and the Lagrange interpolation was used for calculating the percentage of the fat in the samples with a fifth-order polynomial with SSE of 7.6E-30.

Declaration of Competing Interest

The authors declare that they have no known competing financial

Table4
comparisons of the proposed sensor with some previous models.

	Model	MUT	Size (mm^2)	Q-factor	Frequency (GHz)
This work	SRR bent line	Meat	42.5×38	386	3.5
Ref. [6]	SIW Cavity	Ethanol	35×20	$\sim$160	3.2
Ref. [15]	Transmission Line	Oil	70×140	216	6.3
Ref. [22]	Split Ring	Ethanol	30×30	130	2.1
Ref. [23]	Waveguide FSS	Oil	22.8×10.1	291	10.2
Ref. [29]	SRR coupling	Solid dielectric	$\sim$25 $\times$ 25	$\sim$45	2.1
Ref. [30]	SRR Cavity	water	–	$\sim$25	1.95
Ref. [31]	Coupled cavity	Solid dielectric	$\sim$30 $\times$ 30	$\sim$300	2

interests or personal relationships thatcould have appeared to influence the work reported in this paper.

Data availability

Data will be made available on request.

References

[1] M.A. Zidane, A. Rouane, C. Hamouda, H. Amar, Hyper-sensitive microwave sensor based on split ring resonator (SRR) for glucose measurement in water, Sens. Actuators A: Phys. 321 (2021), 112601.

[2] A.A. Helmy, K. Entesari, A 1–8-GHz miniaturized spectroscopy system for permittivity detection and mixture characterization of organic chemicals, IEEE Trans. Microw. Theory Tech. 60 (12) (2012) 4157–4170.

[3] M.A. Aldhaeebi, K. Alzoubi, T.S. Almoneef, S.M. Bamatraf, H. Attia, O.M. Ramahi, Review of microwaves techniques for breast cancer detection, Sensors 20 (8) (2020) 2390.

[4] M.A. Zidane, H. Amar, A. Rouane, Study of two constraints impacting measurements of human glycemia using a microwave sensor, Biosensors 11 (3) (2021) 83.

[5] V.V. Deshmukh, S.S. Chorage, Non-invasive determination of blood glucose level using narrowband microwave sensor, J. Ambient Intell. Humaniz. Comput. (2021) 1–16.

[6] A. Soltan, R. Sadeghzadeh, S. Mohammad-Ali-Nezhad, Microwave sensor for liquid classification and permittivity estimation of dielectric materials, Sens. Actuators A: Phys. (2022), 113397.

[7] B.D. Wiltshire, T. Zarifi, M.H. Zarifi, Passive split ring resonator tag configuration for RFID-based wireless permittivity sensing, IEEE Sens. J. 20 (4) (2019) 1904–1911.

[8] F. Costa, C. Amabile, A. Monorchio, E. Prati, Waveguide dielectric permittivity measurement technique based on resonant FSS filters, IEEE Microw. Wirel. Compon. Lett. 21 (5) (2011) 273–275.

[9] A.K. Jha, M.J. Akhtar, Design of multilayered epsilon-near-zero microwave planar sensor for testing of dispersive materials, IEEE Trans. Microw. Theory Tech. 63 (8) (2015) 2418–2426.

[10] W. Withayachumnankul, K. Jaruwongrungsee, A. Tuantranont, C. Fumeaux, D. Abbott, Metamaterial-based microfluidic sensor for dielectric characterization, Sens. Actuators A: Phys. 189 (2013) 233–237.

[11] F.S. Jafari, F. Kazemi, and J.A. Shokouh, Non-destructive aging of transformer oil using electromagnetic waves, in 2015 20th Conference on Electrical Power Distribution Networks Conference (EPDC), 2015, pp. 277–279: IEEE.

[12] T. Chretiennot, D. Dubuc, K. Grenier, A microwave and microfluidic planar resonator for efficient and accurate complex permittivity characterization of aqueous solutions, IEEE Trans. Microw. Theory Tech. 61 (2) (2012) 972–978.

[13] W. Liu, X. Yang, Y. Niu, H. Sun, Improve planar multiple split-ring sensor for microwave detection applications, Sens. Actuators A: Phys. 297 (2019), 111542.

[14] M.H. Zarifi, M. Rahimi, M. Daneshmand, T. Thundat, Microwave ring resonator-based non-contact interface sensor for oil sands applications, Sens. Actuators B: Chem. 224 (2016) 632–639.

[15] F.S. Jafari, J. Ahmadi-Shokouh, Industrial liquid characterization enhancement using microwave sensor equipped with electronic band gap structure, AEU-Int. J. Electron. Commun. 82 (2017) 152–159.

[16] Z.A. Dijvejin, K.K. Kazemi, K. Alasvand Zarasvand, M.H. Zarifi, K. Golovin, Kirigami-enabled microwave resonator arrays for wireless, flexible, passive strain sensing, ACS Appl. Mater. Interfaces 12 (39) (2020) 44256–44264.

[17] A.M. Gargari, M.H. Zarifi, L. Markley, Passive matched mushroom structure for a high sensitivity low profile antenna-based material detection system, IEEE Sens. J. 19 (15) (2019) 6154–6162.

[18] P. Suneetha, K.S. Naik, P. Muthusamy, Isolation enhancement of metamaterial structure MIMO antenna for WiMAX/WLAN/ITU band applications, Int. J. Microw. Wirel. Technol. (2022) 1–11.

[19] E.L. Chuma, Y. Iano, G. Fontgalland, L.L.B. Roger, H. Loschi, PCB-integrated non-destructive microwave sensor for liquid dielectric spectroscopy based on planar metamaterial resonator, Sens. Actuators A: Phys. 312 (2020), 112112.

[20] Y. Cao, C. Ruan, K. Chen, X. Zhang, Research on a high-sensitivity asymmetric metamaterial structure and its application as microwave sensor, Sci. Rep. 12 (1) (2022) 1–20.

[21] M. Askari, M. Bahadoran, A refractive-index-based microwave sensor based on classical electromagnetically induced transparency in metamaterials, Optik (2022), 168589.

[22] S. Yan, J. Bao, I. Ocket, B. Nauwelaers, G.A. Vandenbosch, Metamaterial inspired miniaturized SIW resonator for sensor applications, Sens. Actuators A: Phys. 283 (2018) 313–316.

[23] F.S. Jafari, J. Ahmadi-Shokouh, Frequency-selective surface to determine permittivity of industrial oil and effect of nanoparticle addition in x-band, J. Electron. Mater. 47 (2) (2018) 1397–1404.

[24] Z. Ghatass, M. Soliman, M. Mohamed, Dielectric technique for quality control of beef meat in the range 10 kHz–1 MHz, Am. -Eurasia J. Sci. Res. 3 (1) (2008) 62–69.

[25] S.K. Ng, et al., Determination of added fat in meat paste using microwave and millimetre wave techniques, Meat Sci. 79 (4) (2008) 748–756.

[26] S.K. Ng, A. Gibson, G. Parkinson, A. Haigh, P. Ainsworth, A. Plunkett, Bimodal method of determining fat and salt content in beef products by microwave techniques, IEEE Trans. Instrum. Meas. 58 (10) (2009) 3778–3787.

[27] S.K. Ng et al., "Characterization of the fat content of beef using microwave techniques," in 2007 European Microwave Conference, 2007, pp. 929–932: IEEE.

[28] M.T. Jilani, W.P. Wen, M.A. Zakariya, and L.Y. Cheong, "Dielectric method for determination of fat content at 1 GHz frequency," in 2014 5th International Conference on Intelligent and Advanced Systems (ICIAS), 2014, pp. 1–4: IEEE.

[29] A. Ebrahimi, J. Scott, K. Ghorbani, Differential sensors using microstrip lines loaded with two split-ring resonators, IEEE Sens. J. 18 (14) (2018) 5786–5793.

[30] A. Ebrahimi, J. Scott, K. Ghorbani, Ultrahigh-sensitivity microwave sensor for microfluidic complex permittivity measurement, IEEE Trans. Microw. Theory Tech. 67 (10) (2019) 4269–4277.

[31] A. Ebrahimi, J. Scott, K. Ghorbani, Transmission lines terminated with LC resonators for differential permittivity sensing, IEEE Microw. Wirel. Compon. Lett. 28 (12) (2018) 1149–1151.

[32] R. Garg, I. Bahl, M. Bozzi, Microstrip Lines And Slotlines, Artech House, 2013.

[33] I.J. Bahl, Lumped Elements for RF and Microwave Circuits, Artech House, 2003.

[34] S.S. Maragheh, M. Dousti, M. Dolatshahi, B. Ghalamkari, Tunable dual-band bandpass filter for multi-standard applications, AEU-Int. J. Electron. Commun. 111 (2019), 152885.

[35] S. Sedighi Maragheh, M. Dousti, M. Dolatshahi, B. Ghalamkari, A dual-mode tunable bandpass filter for GSM, UMTS, WiFi, and WiMAX standards applications, Int. J. Circuit Theory Appl. 47 (4) (2019) 561–571.

[36] S. Shakeri, M. Dousti, and B. Ghalamkari, A quad-band defected microstrip structure loaded bandpass filter for standard GPS, WiFi, WLAN, and WiMAX applications, International Journal of RF and Microwave Computer-Aided Engineering, p. e23082.

[37] B.C. Wadell, Transmission line design handbook. Artech House Microwave Library, 1991.

[38] F. Kazemi, High Q-factor compact and reconfigurable THz aperture antenna based on graphene loads for detecting breast cancer cells, Superlattices Microstruct. 153 (2021), 106865.

[39] V.A. Markel, Introduction to the Maxwell Garnett approximation: tutorial, JOSA A 33 (7) (2016) 1244–1256.

[40] H.-L. Wu, P.-Y. Chen, C.-L. Chi, H.-K. Tsao, Y.-J. Sheng, Vesicle deposition on hydrophilic solid surfaces, Soft Matter 9 (6) (2013) 1908–1919.

Payam Jahangiri was born in Mianeh, Iran in 1989. He received the B.S. degree from Tabriz University, Tabriz, Iran, and M.S. degree from Islamic Azad University, Science and Research Branch, Tehran, Iran, both in electrical engineering, in 2012 and 2015, respectively. He is currently pursuing a Ph.D. degree with the Department of computer and Electrical Engineering, science and research branch, Tehran, Iran. His main research interests include microwave sensors, applied electromagnetics, and antenna design.

M. Naser-Moghadasi was born in Saveh, Iran, In 1959. He received the B.Sc. degree in Communication Eng. in 1985 from the Leeds Metropolitan University (formerly Leeds polytechnic), UK. Between 1985 and 1987 he worked as an RF design engineer for the Gigatech company in Newcastle Upon Tyne, UK. From 1987–1989, he was awarded a full scholarship by the Leeds educational authority to pursue an M.Phil. Studying in CAD of Microwave circuits. He received his Ph.D. in 1993, from the University of Bradford, UK. From 1995, Dr. Naser- Moghadasi joined Islamic Azad University, Science & Research Branch, Iran, where he currently is a Full Professor and head of Computer and Electrical Engineering department. His main areas of interest in research are Microstrip antenna, Microwave passive and active circuits, RF MEMS. He has so far published over 200 papers in different journals and conferences.

Behbod Ghalamkari was born in Tehran, Iran, in 1981. He received the M.Sc. and Ph.D. degrees in electrical engineering from the Amirkabir University of Technology (Tehran Polytechnic), Tehran, Iran in 2007 and 2013, respectively. In 2015, he joined Islamic Azad University, Science and Research Branch, Tehran, Iran, where he is currently an Assistant Professor with the Department of Electrical and Computer Engineering. His current research interests include scattering and inverse scattering in electromagnetic problems, antenna design, and microwave circuits. Dr. Ghalamkari was a recipient of the 2014 ICEE Iranian Conference on Electrical Engineering Prize Paper Award

Massoud Dousti received the B.S. degree in electrical engineering from Orleans University, Orleans, France, in 1991, the M.S. degree in electronics (microwave and optics) from Limoges University, Limoges, France, in 1994, and the Ph.D. degree in electronics (active microwave circuits) from the University of Paris VI, Pierre et Marie Currie, in 1999. He has served as a Teaching Assistant with the Department of Electrical Engineering, Ensea, Cergy Pontoise, France, from 1998 to 2000. In 2001, he joined the Department of Electrical and Computer Engineering, Islamic Azad University, Science and Research Branch, Tehran, Iran, where he is currently an Associate Professor. He is the author of eight books in the field of electronics and translated seven books from English to Farsi in the field of high-frequency, RF MEMS, and MMIC. He is the author and a coauthor of more than 120 published international journal articles and conference papers. His research interests include linear and non-linear RF/microwave/millimeter-wave circuits and systems design, high-frequency electronics (passive and active circuits), RF MEMS, and MMIC technology